Theoretical and Experimental Study of the Vibrational Spectra of the α, β, and δ Phases of Octahydro-1, 3, 5, 7-tetranitro-1, 3, 5, 7-tetrazocine (HMX)

ARTICLE *in* THE JOURNAL OF PHYSICAL CHEMISTRY B · OCTOBER 2002

Impact Factor: 3.3 · DOI: 10.1021/jp020909z

6 AUTHORS, INCLUDING:

Ronald Rabie
Los Alamos National Laboratory
34 PUBLICATIONS **394** CITATIONS
SEE PROFILE

D. J. Funk
Los Alamos National Laboratory
133 PUBLICATIONS **1,485** CITATIONS
SEE PROFILE

Irina Bliss
Parkland Memorial Hospital
6 PUBLICATIONS **145** CITATIONS
SEE PROFILE

Peter Pulay
University of Arkansas
249 PUBLICATIONS **21,370** CITATIONS
SEE PROFILE

Theoretical and Experimental Study of the Vibrational Spectra of the α, *β*, and *δ* Phases of Octahydro-1,3,5,7-tetranitro-1,3,5,7-tetrazocine (HMX)

Holmann V. Brand*

Applied Physics Division, Los Alamos National Laboratory, Los Alamos, New Mexico 87545

Ronald L. Rabie and David J. Funk

Dynamic Experimentation Division, Los Alamos National Laboratory, Los Alamos, New Mexico 87545

Irina Diaz-Acosta and Peter Pulay

Department of Chemistry and Biochemistry, University of Arkansas, Fayetteville, Arkansas 72701

Thomas K. Lippert

Paul Scherrer Institute, 5232 Villigen PSI, Switzerland

Received: April 5, 2002; In Final Form: July 25, 2002

The vibrational spectra of the α, *β*, and *δ* phases of octahydro-1,3,5,7-tetranitro-1,3,5,7-tetrazocine (HMX) have been investigated by complimentary theoretical and experimental approaches. Density functional theory and the scaled quantum mechanical force-field method have been used to calculate the vibrational spectra of the $H_8C_4N_8O_8$ molecule in C_i and C_{2v} symmetry conformations in the gas phase. By comparing the calculated molecular vibrational frequencies of the $H_8C_4N_8O_8$ molecule with the experimental infrared and Raman spectra of HMX crystalline samples, we attempt to assign the intramolecular motions that correspond to the measured bands in the experimental spectra of HMX in α-, *β*-, and *δ*-phase crystal lattices. Our analysis of the vibrational spectra verifies that the particular conformation of the $H_8C_4N_8O_8$ molecule in each crystal lattice of HMX determines, to a great extent, the general pattern of the vibrational spectrum of the crystal lattice. We also compare our detailed motion assignments with the general assignments proposed in previous experimental work. Good agreement is found between the calculated geometry of the $H_8C_4N_8O_8$ molecule in the C_i symmetry conformation and the experimental geometry of molecules in the *β*-phase lattice of HMX and between the calculated geometry of the $H_8C_4N_8O_8$ molecule in the C_{2v} symmetry conformation and the experimental geometry of molecules in the α- and *δ*-phase lattices of HMX.

I. Introduction

The octahydro-1,3,5,7-tetranitro-1,3,5,7-tetrazocine hydrogen-bonded molecular crystal, known as HMX, is a commonly used energetic material in explosives and propellants. HMX is known to exist in three pure crystalline phases, denoted as α, *β*, and *δ*.[1] The infrared (IR) and Raman spectra of HMX have been reported in the literature under various temperatures and pressures in an effort to elucidate the behavior of this energetic material under extreme conditions. Temperature- or pressure-induced changes in the vibrational spectrum of HMX, such as shifting, broadening, and disappearance of spectral bands, have been indicative of phase transformations and chemical reactions.[2−5] Computational studies based on molecular dynamics have confirmed both a dependence of the lattice parameters on temperature[6] and a dependence of the oscillation amplitude of the nitrogen−nitrogen bond on the HMX phase.[7]

Although the detailed mechanisms of chemical decomposition by which energetic materials release energy, when mechanically shocked, are still not well-understood, it has been suggested that these decomposition mechanisms may be the result of transferring thermal and mechanical energy into the internal degrees of freedom of the molecules in energetic materials.[8−10] Hence, it seemed clear to us that characterizing the internal vibrational motion of molecules in energetic materials such as HMX at ambient conditions is an essential, necessary first step that must take place before the complicated changes that are induced in the vibrational spectra by heating or compression can be studied.

The α phase of HMX contains eight $H_8C_4N_8O_8$ molecules per unit cell in an orthorhombic lattice with space group *Fdd*2.[11] The *β* phase contains two $H_8C_4N_8O_8$ molecules per unit cell in a monoclinic lattice with space group $P2_1/c$.[12] The *δ* phase contains six $H_8C_4N_8O_8$ molecules per unit cell in a hexagonal lattice with space group $P6_1$.[13]At ambient conditions, the *β* phase is the most stable form.[2] In the *β*-phase lattice, each $H_8C_4N_8O_8$ molecule has a so-called "chair" conformation (Figure 1a) in which two NO_2 groups are on one side of the C_4N_4 ring and the other two NO_2 groups are on the opposite side of the C_4N_4 ring. This conformation gives the molecule a center of inversion (C_i symmetry). In contrast, each $H_8C_4N_8O_8$ molecule in the α and *δ* phases is in the so-called "boat" conformation (Figure 1b), having all four NO_2 groups on the same side of the C_4N_4 ring. This results in a molecular geometry that almost has C_{2v} symmetry, but the lattice effects slightly distort the C_{2v} molecular symmetry down to C_2 symmetry in the α phase and to C_1 (i.e., no symmetry) in the *δ* phase. It is interesting that the α and *δ* phases, with molecules in the boat conformation, have similar (though not identical) vibrational spectra, whereas the *β* phase, with molecules in the chair conformation, has a significantly different vibrational spectrum.[2−5]

* Corresponding author. E-mail: brand@lanl.gov.

10.1021/jp020909z CCC: $22.00
Published on Web 09/19/2002

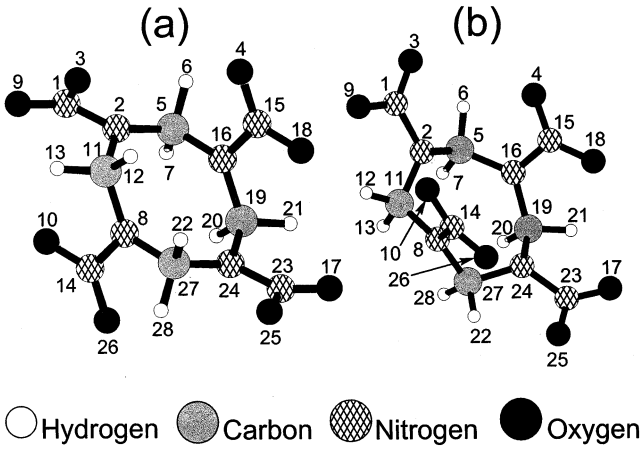

Figure 1. $H_8C_4N_8O_8$ molecule: (a) chair conformation (C_i symmetry); (b) boat conformation (C_{2v} symmetry).

To assign the molecular motions that correspond to measured bands in the experimental vibrational spectra of HMX in α-, *β*-, and *δ*-phase crystal lattices, we use quantum mechanical calculations of the vibrational spectra of the $H_8C_4N_8O_8$ molecule in C_i and C_{2v} symmetry conformations in the gas phase. Our molecular calculations are based on density functional theory and the scaled quantum mechanical (SQM) force-field method. In the future, we hope to be able to relate the changes in the vibrational spectra of HMX that have been induced by heating or compression to the changes in the geometry and composition of the molecules that make up the crystalline material. In this report, we seek to ascertain the molecular motions that make up the vibrational spectra of HMX polymorphs at ambient conditions prior to attempting to understand temperature and pressure effects.

II. Computational Methods

Input geometries for our gas-phase calculations of the $H_8C_4N_8O_8$ molecule were obtained from molecules in the α-, *β*-, and *δ*-phase HMX crystal lattices, built according to the space groups *Fdd*2, $P2_1/c$, and $P6_1$, respectively.[14] We used the quantum mechanical method known as B3-LYP gradient-corrected density functionals with the 6-31G* basis set.[15] The B3-LYP method employs Becke's three-parameter hybrid exchange functional[16] as implemented by Stephens and colleagues[17] and the correlation functional of Lee, Yang, and Parr.[18] Calculations of geometric relaxation and harmonic frequencies using the B3-LYP/6-31G* method were carried out with Gaussian 98 software.[19] B3-LYP/6-31G* calculations are known to agree very well with experimental data.[20−23] The only constraint applied during geometry relaxation was preservation of the point-group symmetry that each molecule had in the crystal lattice, namely, C_2 in the α phase, C_i in the *β* phase, and C_1 in the *δ* phase.

In the SQM force-field procedure,[20] the force-constant matrix, originally calculated in Cartesian coordinates as part of a harmonic frequency calculation, is first transformed into redundant internal valence coordinates (bond lengths, angles, and dihedrals) and is then scaled according to

$$F_{ij}(\text{scaled}) = (S_i S_j)^{1/2} F_{ij} \qquad (2.1)$$

where F_{ij} is the force-constant matrix in redundant internal valence coordinates and S_i and S_j are scaling factors for the redundant internal valence coordinates *i* and *j*, respectively, that denote particular stretches, bends, and torsions. We scaled the F_{ij} matrix by applying the constant scaling factors of Baker and colleagues,[20] which generally produces scaled frequencies close to the experimental values. Using these scaling factors makes it easier to determine which calculated frequency corresponds to which experimental band.

The molecular motion corresponding to each calculated vibrational frequency was determined from an energy distribution analysis[24] and a graphical analysis of the displacements. Both the SQM force-field procedure and the molecular motion analysis were carried out using SCALE computer software distributed by Parallel Quantum Solutions.[25] The resulting description of calculated molecular motions offers more detailed information than experimental techniques and can therefore be used to supplement or refute assignments from experimental efforts.

III. Experimental Section

Fourier transform infrared (FTIR) spectra of the α, *β*, and *δ* polymorphs of HMX were taken using a Bio-Rad FTS-40 spectrometer with 1-cm^{-1} resolution. Sample pellets of KBr were prepared by grinding 0.5 to 1 mg of each polymorph with about 200 mg of dried KBr, using a mortar and pestle, and then pressing the mixture to 20 000 psi with three intensifications. The α and *β* polymorphs were obtained via synthetic routes (U.S. and U.K., respectively). The *δ* polymorph was prepared by heating UK *β*-HMX to 205 °C.

IV. Results

The calculated geometric parameters (X_i-X_j bond lengths, $X_i-X_j-X_k$ angles, and $X_i-X_j-X_k-X_l$ torsions) of the $H_8C_4N_8O_8$ molecule in the C_i and C_{2v} conformations are listed in Tables 1 and 1S (Supporting Information), along with the corresponding values from the experimental X-ray structure of molecules in the α, *β*, and *δ* phases of HMX. The geometric parameters are written in redundant internal valence coordinates (note that all dihedral angles are listed in the Supporting Information, Table 1S). The atom labels are defined according to Figure 1a and b. When available, uncertainty in the experimental geometric parameters is written in parentheses, with one digit in parentheses referring to uncertainty in the last digit, two digits in parentheses referring to uncertainty in the last two digits, etc. As expected, the geometric parameters of the $H_8C_4N_8O_8$ molecule from the α and *δ* phases, originally having C_2 and C_1 symmetry, converged to the same structure with C_{2v} symmetry in the gas-phase calculation of geometric relaxation because the gas-phase calculation does not include the lattice effects that slightly distort the molecule from C_{2v} symmetry.

In general, the calculated geometric parameters were in close agreement with the X-ray data and tended to be near or within the experimental uncertainty limits. The calculated geometric parameters of the molecule in the C_i conformation compare well with the experimental X-ray structure of molecules in the *β* phase. Similarly, the calculated geometric parameters of the molecule in the C_{2v} conformation compare well with the experimental X-ray structure of molecules in the α and *δ* phases. Although some geometric parameters were slightly overestimated and some were slightly underestimated by the theory, when compared to the experimental values, the differences were small. The calculated N−N bond lengths were consistently larger than the corresponding experimental values by 0.02−0.05 Å. However, even in the case of H−C−H angles, which have large experimental uncertainties (up to 15°), there was good agreement between theory and experiment. The worst discrepancies occurred in a couple of isolated cases regarding the

TABLE 1: Geometry of the $H_8C_4N_8O_8$ Molecule in Redundant Internal Valence Coordinates

	chair conformation		boat conformation		
coordinate[a] description	calculated C_i	β crystal[b] C_i	calculated C_{2v}	α crystal[c] C_2	δ crystal[d] C_1
N_2N_1, $N_{24}N_{23}$	1.3923	1.354(5)	1.4145	1.366(12)	1.392(12), 1.365(20)
$N_{14}N_8$, $N_{16}N_{15}$	1.3976	1.373(5)	1.4035	1.353(10)	1.346(25), 1.357(23)
O_3N_1, $O_{25}N_{23}$	1.2302	1.221(8)	1.2227	1.236(10)	1.222(21), 1.212(23)
O_9N_1, $N_{23}O_{17}$	1.2236	1.233(8)	1.2227	1.223(10)	1.202(21), 1.245(22)
$N_{14}O_{10}$, $O_{18}N_{15}$	1.2256	1.205(8)	1.2236	1.237(13)	1.240(12), 1.209(25)
$N_{15}O_4$, $O_{26}N_{14}$	1.2253	1.210(8)	1.2236	1.214(13)	1.250(14), 1.187(23)
C_5N_2, $C_{27}N_{24}$	1.4774	1.473(6)	1.4554	1.448(13)	1.451(21), 1.500(20)
$C_{11}N_2$, $N_{24}C_{19}$	1.4510	1.448(7)	1.4554	1.471(14)	1.486(19), 1.444(24)
$C_{11}N_8$, $C_{19}N_{16}$	1.4608	1.455(6)	1.4505	1.451(14)	1.441(25), 1.473(12)
$N_{16}C_5$, $C_{27}N_8$	1.4416	1.437(6)	1.4505	1.444(13)	1.469(23), 1.476(12)
H_6C_5	1.0884	1.101(15)	1.0867	0.84(09)	1.01
$H_{28}C_{27}$	1.0884	1.101(15)	1.0969	1.07(07)	1.03
H_7C_5	1.0933	1.094(13)	1.0969	1.07(10)	1.08
$C_{27}H_{22}$	1.0933	1.094(14)	1.0867	0.84(15)	1.04
$H_{12}C_{11}$	1.0921	1.110(14)	1.0867	1.07(07)	1.01
$H_{20}C_{19}$	1.0921	1.110(14)	1.0969	0.84(15)	1.11
$H_{13}C_{11}$	1.0894	1.091(14)	1.0969	0.84(15)	1.01
$H_{21}C_{19}$	1.0894	1.091(14)	1.0867	1.07(07)	1.00
$C_5N_2C_{11}$, $C_{19}N_{24}C_{27}$	123.21	122.4(4)	121.14	119.6(1.5)	119.6(0.8), 116.7(1.5)
$C_{11}N_8C_{27}$, $C_5N_{16}C_{19}$	123.59	123.8(4)	124.62	123.7(1.1)	119.3(1.5),121.6(1.4)
$N_2C_5N_{16}$, $N_8C_{27}N_{24}$	111.30	110.1(4)	114.43	113.1(1.5)	112.8(1.6),108.5(1.0)
$N_2C_{11}N_8$, $N_{16}C_{19}N_{24}$	114.23	113.5(4)	114.43	110.5(1.5)	113.0(1.5),112.6(1.3)
$H_6C_5H_7$, $H_{22}C_{27}H_{28}$	108.78	109.7(11)	109.64	112(13)	102, 135
$H_{12}C_{11}H_{13}$, $H_{20}C_{19}H_{21}$	109.43	106.2(9)	109.64	110(15)	128, 107
$O_3N_1O_9$, $O_{17}N_{23}O_{25}$	126.76	125.9(6)	126.41	124.9(1.7)	127.3(1.0),121.4(1.7)
$O_{10}N_{14}O_{26}$, $O_4N_{15}O_{18}$	127.37	126.7(5)	127.54	124.8(1.7)	122.8(1.9),126.0(1.8)
$N_2N_1O_3$, $N_{24}N_{23}O_{25}$	115.13	116.2(5)	116.79	118.0(1.6)	116.2(1.3), 120.4(1.5)
$N_2N_1O_9$, $O_{17}N_{23}N_{24}$	118.05	117.9(5)	116.79	117.2(1.6)	116.6(1.4), 117.6(1.5)
$N_8N_{14}O_{10}$, $N_{16}N_{15}O_{18}$	115.88	117.5(5)	116.23	116.4(1.5)	115.0(1.6), 119.9(1.1)
$N_8N_{14}O_{26}$, $O_4N_{15}N_{16}$	116.73	115.9(5)	116.23	118.8(1.5)	122.1(1.1), 114.1(1.7)
$N_1N_2C_5$, $N_{23}N_{24}C_{27}$	114.44	115.1(4)	117.86	119.6(1.5)	120.7(1.3), 118.6(1.3)
$N_1N_2C_{11}$, $C_{19}N_{24}N_{23}$	118.16	118.2(4)	117.86	119.3(1.5)	118.6(1.2), 119.4(1.2)
$C_{11}N_8N_{14}$, $N_{15}N_{16}C_{19}$	117.89	117.4(4)	117.41	119.2(1.1)	123.5(1.0), 117.7(1.4)
$N_{14}N_8C_{27}$, $C_5N_{16}N_{15}$	118.10	118.2(4)	117.41	116.9(1.4)	117.2(1.4), 120.8(0.9)
$N_2C_5H_6$	108.53	109.2(7)	107.18	107(7)	109
$N_{24}C_{27}H_{28}$	108.53	109.2(7)	109.85	108(6)	110
$N_2C_5H_7$	110.07	110.1(8)	109.85	108(6)	103
$H_{22}C_{27}N_{24}$	110.07	110.1(8)	107.18	107(7)	101
$H_6C_5N_{16}$	109.90	110.5(7)	109.60	112(7)	109
$N_8C_{27}H_{28}$	109.90	110.5(7)	106.11	106(6)	108
$H_7C_5N_{16}$	108.23	107.3(8)	106.11	106(6)	120
$N_8C_{27}H_{22}$	108.23	107.3(8)	109.60	112(7)	91
$N_2C_{11}H_{12}$	109.81	108.5(7)	107.18	105(5)	107
$H_{20}C_{19}N_{24}$	109.81	108.5(7)	109.85	107(9)	110
$N_2C_{11}H_{13}$	106.20	109.8(7)	109.85	107(9)	109
$H_{21}C_{19}N_{24}$	106.20	109.8(7)	107.18	105(5)	109
$N_8C_{11}H_{12}$	105.92	106.6(7)	109.60	111(6)	92
$N_{16}C_{19}H_{20}$	105.92	106.6(7)	106.11	112(9)	110
$N_8C_{11}H_{13}$	111.24	111.8(7)	106.11	112(9)	108
$N_{16}C_{19}H_{21}$	111.24	111.8(7)	109.60	111(6)	108

[a] Atom labels are defined according to Figure 1a and b. Bond lengths are in angstroms, and angles, in degrees. [b] Ref 12. [c] Ref 11. [d] Ref 13.

H−C−H angles; in these, the calculated C_{2v} values were smaller than the experimental δ-phase values by 15−18°. These discrepancies were near the estimated experimental uncertainty. If we consider that the calculated geometric parameters are for a molecule in the gas phase, whereas the experimental geometric parameters are for molecules in crystal lattices, the overall good agreement between the calculated and experimental geometric parameters seems remarkable.

Our calculated and measured vibrational spectra of HMX are listed in Tables 2 and 3 and shown in Figures 2 and 3. In addition to listing our own experimental IR spectra of HMX polymorphs, we also list previously reported IR and Raman spectral bands[2,4,5] in Tables 2 and 3. Table 2 lists the 78 calculated frequencies, IR intensities (in km/mol), and Raman activities (in Å^4/amu) of the $H_8C_4N_8O_8$ molecule in the C_i symmetry conformation as well as the experimentally observed IR and Raman bands of the β phase of HMX. Similarly, Table 3 lists the 78 calculated frequencies, IR intensities, and Raman activities of the $H_8C_4N_8O_8$ molecule in the C_{2v} symmetry conformation as well as the experimentally observed IR and Raman bands of the α and δ phases of HMX. To facilitate a comparison with the experimental data, the calculated IR intensities shown in Figures 2 and 3 were broadened with a Lorentzian shape of 4-cm^{-1} width, and the scale of the intensity coordinate was made arbitrary.

The one-to-one correspondence between the calculated IR-active frequencies and the experimental IR bands (shown in Tables 2 and 3) was based on similarities in both their frequency magnitudes and IR intensity patterns. This correspondence between calculated and measured IR bands, in turn, enabled us to infer a correspondence between calculated and measured Raman bands on the basis of similar frequency magnitudes.

TABLE 2: Vibrational Spectrum of the $H_8C_4N_8O_8$ Molecule in the C_i Conformation

		calculated[a] C_i molecule			experiment[b] β crystal				
					IR			Raman	
mode	description[c]	IR int.	Raman act.	freq. cm^{-1}	this work	ref 2	ref 5	ref 4	ref 5
1	b(N···NN)	4.3	0.0	15					
2	b(N···NN)	6.8	0.0	51					
3	b(N···NN)	0.0	4.3	60					
4	t(NCNN)	1.4	0.0	64					
5	b(N···NN)	0.0	2.0	66					
6	$\gamma_{NN}(NO_2)$	0.0	2.0	87					
7	$\gamma_{NN}(NO_2)$	0.3	0.0	92					
8	$\gamma_{NN}(NO_2)$	0.0	2.6	115					
9	$\gamma_{NN}(NO_2)$	0.6	0.0	125					
10	σ(CNC)	0.0	1.7	154					
11	b(NNC)	9.6	0.0	166					
12	σ(CNC)	21.9	0.0	206					
13	b(NNC), b(CNC)	0.0	2.9	217					
14	b(NNC), b(NCN)	0.0	1.6	270					
15	b(NNC), b(NNO)	0.0	0.5	299					
16	b(NNC)	9.3	0.0	337					
17	ν(CN), ν(NN), b(NCN)	0.0	6.8	342					
18	ν(NN), b(CNC), b(NNC)	6.2	0.0	371					
19	b(NNO), b(NNC)	0.0	4.5	399				412	417
20	b(NNO), b(NNC)	7.5	0.0	402	419		420		
21	b(CNC), b(NNC)	0.0	3.2	420				432	437
22	b(CNC), b(NNO), b(NNC)	5.9	0.0	425	438		441		
23	b(NNO)	40.0	0.0	594	600		605		
24	b(NNO)	0.0	4.8	594				597	600
25	b(NNO), ν(NN)	31.9	0.0	622	627		630		
26	b(NNO), ν(NN)	0.0	6.3	625				638	640
27	b(NNO), ν(NN)	7.7	0.0	644		660	658		
28	b(NNO), ν(NN)	0.0	3.5	650				662	663
29	b(ONO), ν(CN)	0.0	1.8	726				721	722
30	σ(ONO)	20.5	0.0	740	754	752	755		
31	σ(ONO)	0.0	0.3	741				759	762
32	σ(ONO)	0.0	0.2	745					763
33	σ(ONO)	36.2	0.0	746	760	758	762		
34	b(NCN)	12.9	0.0	778	772	769*	773*		
35	$\nu_s(NC_2)$	0.0	21.3	826				834	834
36	$\nu_s(NC_2)$	5.5	0.0	828	832[d]	827	833		
37	$\nu_s(NNC_2)$	15.0	0.0	862	872	871	872		
38	$\nu_s(NNC_2)$	0.0	9.3	872				881	884
39	$\nu_{as}(NNC_2)$	272.8	0.0	922	947	945	948		
40	ν(NN), $\rho(CH_2)$	0.0	20.7	925				950	953
41	ν_{as}(CNN), $\rho(CH_2)$	0.0	2.4	936				965	966
42	ν_{as}(CNN), $\rho(CH_2)$	256.5	0.0	937	967	965	966		
43	ν(NN), $\rho(CH_2)$	107.6	0.0	1057	1088	1090	1089		
44	$\nu_{as}(NNC_2)$	0.0	7.0	1061				1090	1088
45	ν_{as}(CNN), $\rho(CH_2)$	161.0	0.0	1137	1146	1146	1145		
46	ν_{as}(CNN), $\rho(CH_2)$	0.0	6.7	1167				1168	1170
47	$\nu_{as}(NC_2)$	0.0	10.6	1197				1190	1192
48	$\nu_{as}(NC_2)$	163.8	0.0	1213	1204	1205	1203		
49	$\nu_{as}(NC_2)$	54.4	0.0	1236	1239	1240			
50	$\nu_{as}(NC_2)$	0.0	3.7	1238				1248*	1251*
51	$\nu_s(NO_2)$	0.0	17.4	1272				1268	1270
52	$\nu_s(NO_2)$	961.2	0.0	1280	1279	1280	1281		
53	$\nu_s(NO_2)$	498.9	0.0	1294	1296sh		1298		
54	$\gamma(CH_2)$	0.0	11.8	1311				1312*	1310*
55	$\nu_s(NO_2)$	0.0	20.2	1322					1318
56	$\gamma(CH_2)$	28.5	0.0	1323	1325	1320*	1325*		
57	$\gamma(CH_2)$	17.3	0.0	1347	1349	1348*	1348*		
58	$\gamma(CH_2)$	0.0	19.7	1348				1350*	1351*
59	$\omega(CH_2)$	0.0	9.9	1369				1368	1369
60	$\omega(CH_2)$	39.0	0.0	1397	1385	1397	1395		
61	$\omega(CH_2)$	28.6	0.0	1404	1395		1401		
62	$\omega(CH_2)$	0.0	9.0	1422				1418	1420
63	b(HCH)	0.0	8.8	1446				1438	1438
64	b(HCH)	35.3	0.0	1448	1433	1433	1434		
65	b(HCH)	0.0	17.8	1461				1460	1461
66	b(HCH)	109.5	0.0	1464	1462	1465	1463		
67	$\nu_{as}(NO_2)$	0.0	1.9	1611				1532	1535
68	$\nu_{as}(NO_2)$	517.1	0.0	1615	1534	1540	1538		
69	$\nu_{as}(NO_2)$	0.0	3.1	1624				1558	1560
70	$\nu_{as}(NO_2)$	550.5	0.0	1626	1563	1570	1565		
71	$\nu_s(CH_2)$	0.0	33.5	2966					
72	$\nu_s(CH_2)$	8.4	0.0	2967	2985[e]		2978		
73	$\nu_s(CH_2)$	28.5	0.0	2982	2992sh		2983		
74	$\nu_s(CH_2)$	0.0	202.2	2983				2992	2994
75	$\nu_{as}(CH_2)$	0.0	47.2	3046				3028	3028
76	$\nu_{as}(CH_2)$	4.5	0.0	3046	3027		3027		
77	$\nu_{as}(CH_2)$	7.2	0.0	3049	3037		3037		
78	$\nu_{as}(CH_2)$	0.0	90.0	3049				3037	3038

[a] All frequencies are in cm^{-1}. Calculated IR intensities and Raman activities are in km/mol and $Å^4$/amu, respectively. The $H_8C_4N_8O_8$ molecule in the C_i conformation is shown in Figure 1a. [b] Shoulders are marked "sh". Experimental bands whose previous assignments we question on the basis of the calculated motions are marked with an asterisk. [c] b(XYZ): bend of X−Y−Z angle; b(N···NN): bend in which N···N atoms are on opposite sides of the ring and are related by inversion symmetry; r.d.: ring deformation; $\gamma(XY_2)$: twist about bisector of Y−X−Y angle; $\gamma_{NN}(XY_2)$: twist of XY_2 about NN bond; $\omega(XY_2)$: wag of Y_2 atoms out of XY_2 plane; $\sigma(XY_2)$: wag of X atom out of XY_2 plane; $\rho(XY_2)$: rocking in XY_2 plane; $\nu_{as}(XY_2)$: asymmetric stretch of Y−X−Y bonds; $\nu_{as}(XXY_2)$: asymmetric stretch of X−X−Y_2 bonds; $\nu_s(XY_2)$: symmetric stretch of Y−X−Y bonds; $\nu_s(XXY_2)$: symmetric stretch of X−X−Y_2 bonds; t: torsion. [d] This band appears to have a shoulder around 839 cm^{-1}. [e] Five IR bands were observed in the ν(CH) region of β-HMX: 2925, 2985, 2992sh, 3027, and 3037 cm^{-1}.

TABLE 3: Vibrational Spectrum of the $H_8C_4N_8O_8$ Molecule in the C_{2v} Conformation

		calculated[a]			experiment[b]					
					α crystal			δ crystal		
		C_{2v} molecule			IR		Raman	IR		Raman
mode	description[c]	IR int.	Raman act.	freq. cm^{-1}	this work	ref 2	ref 4	this work	ref 2	ref 4
1	b(N···NN)	0.0	0.7	28						
2	b(N···NN)	2.8	1.7	48						
3	t(NCNN)	0.0	0.3	53						
4	b(N···NN)	0.0	3.8	54						
5	b(N···NN)	0.1	0.8	70						
6	$\gamma_{NN}(NO_2)$	0.0	2.5	90						
7	$\gamma_{NN}(NO_2)$	0.1	0.3	95						
8	$\gamma_{NN}(NO_2)$	0.0	0.6	103						
9	$\gamma_{NN}(NO_2)$	0.0	0.9	103						
10	σ(CNC)	0.1	0.4	129						
11	b(NNC)	7.5	0.8	189						
12	σ(CNC)	0.5	0.4	194						
13	b(CNC)	0.4	2.1	216						
14	b(NNC), b(CNC)	0.0	1.3	255						
15	b(NNC)	0.0	0.1	329						
16	ν(CN), ν(NN), b(NCN)	2.2	8.6	358						
17	ν(NN), ν(CN), b(CNC)	9.7	0.1	377						
18	ν(NN), b(NNO)	0.0	0.0	396						
19	b(NNC), b(NNO), $\rho(CH_2)$	16.1	0.7	404						
20	b(NNO), b(NNC), $\rho(CH_2)$	0.0	4.9	408				400		392
21	b(NNO), b(NNC), $\rho(CH_2)$	0.0	0.5	444						446
22	b(CNC), $\rho(CH_2)$	5.6	1.9	464	451		450	470		473
23	b(NNO)	0.0	2.4	584						590
24	b(NNO)	49.9	0.5	592	603	603	594	599	605	601
25	b(NNO), ν(NN)	12.3	4.8	611	622	625	620	621	625	622
26	ν(NN), b(ONO)	0.2	0.2	631						
27	ν(NN), b(ONO)	2.1	6.8	633	646	648	646	646	655	654
28	b(NNO), b(NNC), ν(CN)	0.0	0.0	635						
29	ν(NN), b(ONO)	11.8	2.8	704	714	714	712	711	713	713
30	σ(ONO)	34.7	0.7	727	741	742	740	733	740	735
31	σ(ONO)	5.2	0.1	737	751	753	750	750	750	751
32	σ(CNC)	8.9	1.9	744			758*			763*
33	σ(ONO)	35.2	0.0	745	766	768		763	765	
34	σ(ONO)	5.4	0.6	751	770			767		
35	$\nu_s(NC_2)$	24.7	15.7	828				830		
36	$\nu_s(NC_2)$	35.3	0.2	836	847	848	846	841	848	846
37	b(ONO), $\nu_s(NNC_2)$	0.2	0.3	864	864	862		867	866	870
38	b(ONO), $\nu_s(NNC_2)$	4.2	4.9	869	878		878			
39	b(ONO), $\nu_s(NNC_2)$	605.8	0.0	883	915			913	910	
40	$\nu_s(NNC_2)$	170.7	0.0	906		920	928	930	925	930
41	ν(NN), b(ONO)	82.3	21.2	910	944	945	945	941	940	943
42	ν(CN), $\rho(CH_2)$	0.0	2.6	918						
43	$\nu_s(NNC_2)$	123.2	0.6	989	1030	1032	1030	1016	1040	
44	$\nu_s(NNC_2)$, $\rho(CH_2)$	51.1	2.6	1062	1089	1090	1085	1087	1088	1092
45	$\nu_s(NNC_2)$, $\rho(CH_2)$	25.7	3.7	1097	1109	1110		1109	1110	1111
46	$\nu_{as}(NC_2)$	0.0	0.0	1150	1148sh			1147sh		
47	$\nu_{as}(NC_2)$	116.4	0.1	1207	1215	1220*	1215	1204	1215*	
48	ν(NO), ν(NN), b(CNC)	47.6	17.0	1223				1222		1225*
49	$\nu_{as}(NC_2)$	0.0	4.3	1249						
50	$\nu_{as}(NC_2)$	457.3	1.1	1251	1259		1258*	1249		
51	$\nu_s(NO_2)$	29.9	7.1	1269	1268			1257		1256
52	$\nu_s(NO_2)$	372.1	0.9	1275	1280sh[d]	1280	1280	1274	1270	1275
53	$\nu_s(NO_2)$	77.4	8.9	1293				1290		1291
54	$\gamma(CH_2)$	0.0	1.5	1321						
55	$\nu_s(NO_2)$	355.9	22.7	1327	1319	1320	1318	1320	1325	1317
56	$\gamma(CH_2)$	19.4	9.9	1339				1341	1340*	1332*
57	$\omega(CH_2)$	0.0	1.0	1360						
58	$\gamma(CH_2)$	0.8	9.0	1378	1364					
59	$\gamma(CH_2)$	2.3	7.3	1382	1370	1370	1368	1370	1370	1371
60	$\omega(CH_2)$	12.0	13.1	1387	1386		1385	1383		1382
61	$\omega(CH_2)$	44.8	5.7	1404	1393	1394	1391	1395	1393	1393
62	b(HCH)	0.0	11.1	1422						
63	$\omega(CH_2)$	6.4	3.9	1423	1414	1416	1412	1419	1420	1415
64	b(HCH)	0.9	1.0	1433	1432	1432	1422			1422
65	b(HCH)	22.5	7.4	1447			1448			1442
66	b(HCH)	124.3	5.0	1454	1451	1468		1451	1455	
67	$\nu_{as}(NO_2)$	0.0	0.2	1545						
68	$\nu_{as}(NO_2)$	538.0	0.0	1564	1541		1539	1545		1536
69	$\nu_{as}(NO_2)$	516.3	0.6	1567	1561	1550	1561	1562	1560	1562
70	$\nu_{as}(NO_2)$	0.0	6.1	1573						
71	$\nu_s(CH_2)$	5.2	0.8	2927						
72	$\nu_s(CH_2)$	0.0	1.0	2927						
73	$\nu_s(CH_2)$	5.8	14.8	2937						
74	$\nu_s(CH_2)$	78.3	275.1	2941	2970		2975	2970		2974
75	$\nu_{as}(CH_2)$	0.0	23.7	3067			3047			
76	$\nu_{as}(CH_2)$	33.5	1.3	3069	3049			3058		
77	$\nu_{as}(CH_2)$	6.2	0.1	3069	3056				3058	
78	$\nu_{as}(CH_2)$	1.3	89.6	3071			3053			3058

[a] All frequencies are in cm^{-1}. Calculated IR intensities and Raman activities are in km/mol and $Å^4$/amu, respectively. The $H_8C_4N_8O_8$ molecule in the C_{2v} conformation is shown in Figure 1b. [b] Shoulders are marked "sh". Experimental bands whose previous assignments we question on the basis of the calculated motions are marked with an asterisk. [c] b(XYZ): bend of X−Y−Z angle; b(N···NN): bend in which N···N atoms are on opposite sides of the ring and are related by inversion symmetry; r.d.: ring deformation; $\gamma(XY_2)$: twist about bisector of Y−X−Y angle; $\gamma_{NN}(XY_2)$: twist of XY_2 about NN bond; $\omega(XY_2)$: wag of Y_2 atoms out of XY_2 plane; $\sigma(XY_2)$: wag of X atom out of XY_2 plane; $\rho(XY_2)$: rocking in XY_2 plane; $\nu_{as}(XY_2)$: asymmetric stretch of Y−X−Y bonds; $\nu_{as}(XXY_2)$: asymmetric stretch of X−X−Y_2 bonds; $\nu_s(XY_2)$: symmetric stretch of Y−X−Y bonds; $\nu_s(XXY_2)$: symmetric stretch of X−X−Y_2 bonds; t: torsion. [d] This is only an estimate because this shoulder is unresolved in our IR spectra.

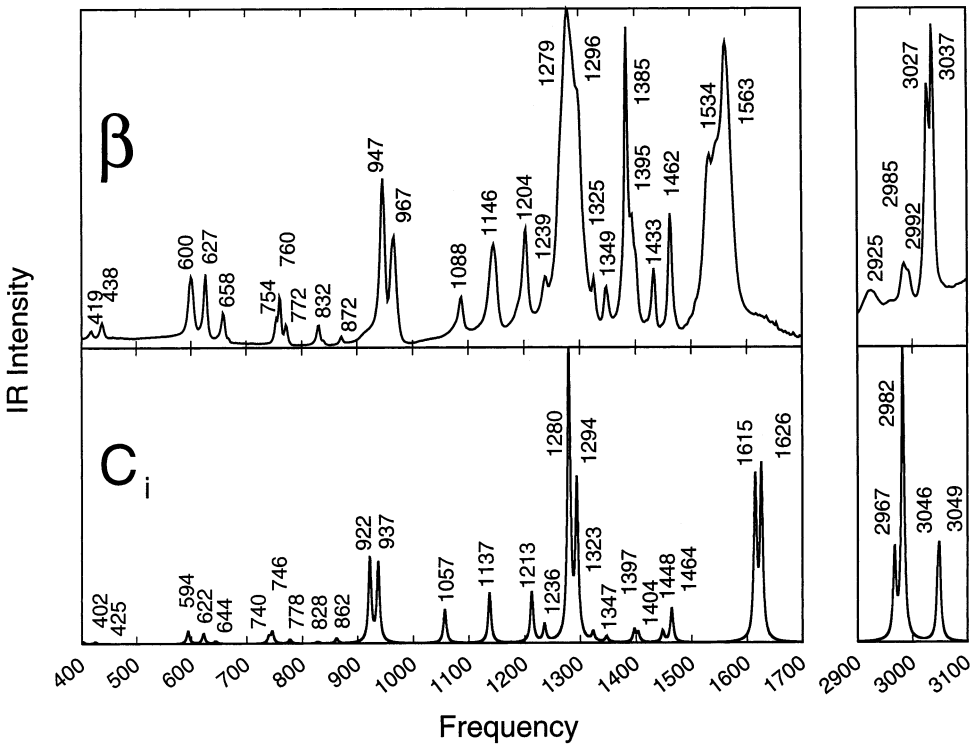

Figure 2. Calculated IR spectrum of the $H_8C_4N_8O_8$ molecule in the C_i conformation and measured IR spectrum of the β phase of HMX.

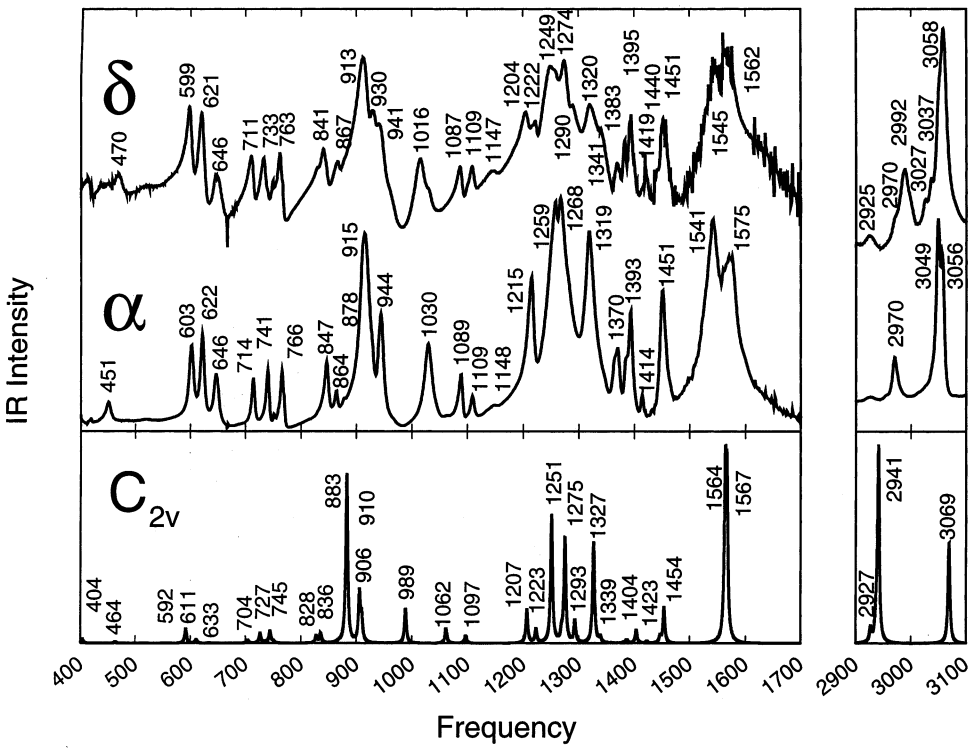

Figure 3. Calculated IR spectrum of the $H_8C_4N_8O_8$ molecule in the C_{2v} conformation and measured IR spectra of the α and δ phases of HMX.

Thus, we were able to ascribe the calculated molecular motion to the experimental IR and Raman bands. Therefore, the motion of the calculated frequencies allowed us either to confirm or question previous experimental assignments of the IR and Raman bands of the α, β, and δ phases of HMX on the basis of frequency shifts observed when using isotope substitutions.[2,4,5] Those bands whose previous assignments we question have been marked with an asterisk in Tables 2 and 3. We did not attempt to establish a one-to-one correspondence between calculated and measured frequencies below 400 cm^{-1}, partly because our measured IR spectra did not span that region and partly because that low-frequency region may include interspersed lattice phonons, which are not included in our calculations of a single $H_8C_4N_8O_8$ molecule in the gas phase.

The calculated and measured frequencies are in reasonable agreement. This agreement is encouraging because our calculated frequencies are for a molecule in the gas phase and include neither effects due to intermolecular hydrogen bonding present

in the crystal lattice nor effects due to Fermi resonance, which are present in the experimental data. The largest difference between the calculated and measured frequencies was 81 cm^{-1} in the β phase, 41 cm^{-1} in the α phase, and 41 cm^{-1} in the δ phase. As shown in Table 2, the calculated frequencies of the $H_8C_4N_8O_8$ molecule in the C_i symmetry conformation generally agree with the experimental bands of β-HMX, within 32 cm^{-1}, except for the four modes corresponding to asymmetric stretches of NO_2 moieties, denoted $\nu_{as}(NO_2)$, where the calculated frequencies were higher than the experimental values by 63−81 cm^{-1}. Because this somewhat large 63−81-cm^{-1} discrepancy between the calculated and experimental frequencies occurred only in the β phase and was not found in any of the frequencies in the α and δ phases (Table 3), this discrepancy appears to be an isolated instance specific to intermolecular interactions afforded by the lattice of the β phase. Hence, other than this isolated difference in the four $\nu_{as}(NO_2)$ modes of the β phase, the calculated frequencies seem to be in general agreement with the experimental data, within 41 cm^{-1} for all three phases of HMX.

A comparison between our calculated and measured IR spectral plots (Figures 2 and 3) verifies that the conformation of the $H_8C_4N_8O_8$ molecule in a particular crystal phase is, in fact, a determining factor in the vibrational pattern of the crystal phase. The β phase, where the $H_8C_4N_8O_8$ molecules are in the chair (C_i symmetry) conformation, has an IR spectrum that resembles the calculated IR spectrum of the $H_8C_4N_8O_8$ molecule in the C_i symmetry conformation, and it differs from the IR spectra of the α and δ phases, where the $H_8C_4N_8O_8$ molecules are in the boat conformation. The α and δ phases have similar, though not identical, IR spectra because their $H_8C_4N_8O_8$ molecules are in a similar boat conformation, which is slightly distorted from C_{2v} symmetry in a unique manner by the lattice of each phase (Table 1).

We now scrutinize our calculated and measured IR spectra (Tables 2 and 3 and Figures 2 and 3) in individual regions of the frequency spectrum starting with the lowest frequency region and progressing to higher frequency regions. We will henceforth refer to the calculated frequency spectrum of the $H_8C_4N_8O_8$ molecule in the conformation with either C_i or C_{2v} symmetry as simply the spectrum of C_i or C_{2v}. The experimental spectra of the α, β, and δ phases of HMX are referred to as simply the spectra of α, β, and δ. In our discussion, the calculated and measured frequencies will be explicitly labeled either IR or Raman because Tables 2 and 3 show previously reported experimental IR[2,5] and Raman bands[4,5] of α, β, and δ in addition to our own experimental IR spectra. Also note that the frequencies of C_i can only be either IR active or Raman active, whereas the frequencies of C_{2v} can be both IR and Raman active. Frequencies that are IR active will be referred to as IR frequencies, and frequencies that are Raman active will be referred to as Raman frequencies. The suffix "sh" attached to a vibrational frequency magnitude denotes "shoulder."

Region 400−500 cm^{-1}. C_i and C_{2v} have four frequencies in this region. C_i has two low-intensity IR frequencies and two Raman frequencies that agree with the IR and Raman bands of β, within 18 cm^{-1}. C_{2v} has two frequencies that are both IR and Raman active and two frequencies that are only Raman active. The four frequencies of C_{2v} agree with the IR and Raman bands of α, within 14 cm^{-1}, and with those of δ, within 16 cm^{-1}. In agreement with the general assignments proposed previously in refs 2, 4, and 5, we find that the motion corresponding to the frequencies in this region is concentrated in distortions of the C_4N_4 ring.

Region 500−700 cm^{-1}. Three frequencies near 600 cm^{-1} are well-resolved in all the calculated and experimental IR spectra in this region. This region is unique in that the three IR bands look so similar in α, β, and δ that it is difficult to distinguish among the phases. The first two bands are of comparable intensity, and the third one is of lower intensity in the spectra of all three phases. In α, the second band is slightly more intense than the first one, whereas in β and δ, the first and second bands have about the same IR intensity. The three IR frequencies in both C_i and C_{2v} have intensities that decrease monotonically with increasing frequency, but the intensities of the frequencies in C_{2v} decrease faster. With regard to IR intensities, the calculated and experimental values agree only in that the third frequency has the lowest intensity. However, with regard to frequency values, the three IR frequencies in C_i are in excellent agreement with the three IR bands of β, deviating by as little as 5−14 cm^{-1}. Similarly, the three IR frequencies in C_{2v} agree quite well with the three IR bands of α, within 5−13 cm^{-1}, and with the three IR bands of δ, within 7−13 cm^{-1}.

The molecular motion of the three IR frequencies of C_i and the first two IR frequencies of C_{2v} in this region is mostly concentrated in the bending of N−N−O angles, denoted b(NNO), and the stretching of N−N bonds, denoted ν(NN). The third IR frequency of C_{2v} in this region includes ν(NN) and the bending of O−N−O angles, denoted b(ONO). In agreement with the calculated motions, previous experimental work assigned the three IR bands in α, β, and δ in this region to general ring distortions and deformations involving one ring bond and one nonring bond associated with the NO_2 functional groups.[2,5] The Raman frequencies of C_i in this region (594, 625, and 650 cm^{-1}) agree with the Raman bands of β (Table 2) reported in ref 4, within 3−13 cm^{-1}, and with those reported in ref 5, within 6−15 cm^{-1}. The motion of the first of these three Raman frequencies of C_i is concentrated in b(NNO), whereas the motion of the next two Raman frequencies is concentrated in b(NNO) and also in ν(NN). These calculated motion descriptions are consistent with those proposed in refs 4 and 5, where the three Raman bands of β in this region were assigned the same motion as the three IR bands of β in the same region.[2] Of the five Raman frequencies of C_{2v} (584, 592, 611, 631, and 633 cm^{-1}), the 584 cm^{-1} frequency does not appear to correspond to any reported Raman band in α, and the 631 cm^{-1} frequency does not appear in either α or δ. The remaining Raman frequencies of C_{2v} in this region do agree with the reported experimental Raman bands, within 2−13 cm^{-1} in α and within 6−21 cm^{-1} in δ.[4] The motion of the five Raman bands of C_{2v} in this region is concentrated in the NO_2 moiety (Table 3), which is consistent with the assignments of the earlier experimental report given in ref 4.

Region 700−800 cm^{-1}. In Figures 2 and 3, the calculated IR spectra of C_i and C_{2v} show clear differences in this region. Concurrently, α and δ share similarities in both IR intensity and band separation, whereas β has a significantly different IR spectral pattern. The three IR frequencies of C_i (740sh, 746, and 778 cm^{-1}) have an intensity pattern similar to that of the three IR bands of β (754sh, 760, and 772 cm^{-1}), where the second band is the most intense of the three and the third band is the least intense. The IR intensity pattern of the four frequencies of C_{2v} (704, 727, 737sh, and 745 cm^{-1}) resembles that of the four IR bands of α (714, 741, 751sh, and 766 cm^{-1}), where the first band is less intense than the second and fourth, both of which have comparable intensity. However, of the four IR bands in δ (711, 733, 750sh, and 763 cm^{-1}), the first and second have about the same intensity, in contrast to the intensity

pattern of the frequencies in C_{2v}. The frequency 737sh cm^{-1} in the calculated IR spectrum of C_{2v} appears in α at 751 cm^{-1} and in δ at 750 cm^{-1}, appearing as well-resolved shoulders in both IR spectra. In C_{2v}, the low-intensity IR frequencies 744 and 751 cm^{-1} that flank the more intense frequency 745 cm^{-1} may correspond to the unresolved shoulders on both sides of the 766 cm^{-1} IR band in α and the 763 cm^{-1} IR band in δ. Because of the one-to-one correspondence between the three calculated IR frequencies of C_i and the three IR bands of β, we may confidently assign the following calculated motion to these experimental IR bands: wagging the N atoms out of the NO_2 planes, denoted σ(ONO), to our IR bands 754 and 760 cm^{-1} and bending the N−C−N angles in the C_4N_4 ring, to our 772 cm^{-1} IR band in β. In addition to the three IR-active frequencies of C_i, there are also three Raman-active frequencies of C_i (726, 741, and 745 cm^{-1}) in this region. The first two agree with the two Raman bands of β (Table 2) reported in ref 4, within 5 and 18 cm^{-1}, respectively, and all three calculated Raman frequencies agree with the three Raman bands of β reported in ref 5, within 1, 21, and 18 cm^{-1}, respectively.

Of the six frequencies of C_i in this region, the lowest frequency (726 cm^{-1} Raman-active) and the highest frequency (778 cm^{-1} IR-active) include the motion of ring atoms such as ν(CN) and b(NCN), respectively. The other four frequencies (two IR-active and two Raman-active) have their motion concentrated in σ(ONO). Our motion assignments for β are consistent with those of refs 4 and 5, which assigned the distortion of NO_2 moieties and general ring distortions to the first Raman band (726 cm^{-1}) and the distortion of only NO_2 moieties to the rest of the Raman bands in this region. Our motion assignments in this region are also consistent with those of ref 2, which were general deformations involving one ring bond and one nonring bond belonging to the NO_2 moieties for the IR bands of β. An exception was the highest frequency (778 cm^{-1}), for which they did not include ring deformation in their assignment.

There are also six frequencies of C_{2v} in this region. All six frequencies have IR intensities, and five of them have Raman activities. The motion of five of these six frequencies is concentrated in NO_2 moieties such as b(ONO) and σ(ONO). The fourth frequency (744 cm^{-1}) involves a ring distortion composed of the wagging of N atoms out of the CNC planes (σ(CNC)). In this region, our IR spectra show four bands in α and δ that are very similar to the four IR bands reported in ref 2. There were also four Raman bands in α and δ reported in ref 4. In this region, the calculated motion of the frequencies of C_{2v} agrees with those proposed in refs 2 and 4 for IR and Raman bands of α and δ, except for the first frequency (704 cm^{-1} of C_{2v}), to which we assign ν(NN) and b(ONO), whereas refs 2 and 4 assigned a general ring deformation.

Region 800−970 cm^{-1}. The IR spectra of α, β, and δ display unique features in this region, clearly distinguishing one phase from another. Their IR spectra have in common, however, the fact that each has a set of lower-frequency bands with low intensities and a set of higher-frequency bands with high intensities. In the higher-frequency, high-intensity set of IR bands, in β we see two sharp bands at 947 and 967 cm^{-1}, in α we see one somewhat broad band at 915 cm^{-1} and one sharp band at 944 cm^{-1}, and in δ we see one broad band at 913 cm^{-1} with two shoulders at 930 and 941 cm^{-1}. The IR spectra of C_i and C_{2v} also have a set of lower frequencies with low intensities and a set of higher frequencies with high intensities. In the higher-frequency, high-intensity set of IR frequencies, there are two frequencies at 922 and 937 cm^{-1} in C_i and three frequencies at 883, 902, and 910 cm^{-1} in C_{2v}. In C_i, the 922 cm^{-1} frequency is only slightly more intense than the 937 cm^{-1} frequency, whereas in C_{2v}, the 883 cm^{-1} frequency is much more intense than the 902- and 910-cm^{-1} frequencies. The high-intensity 922 and 937 cm^{-1} IR frequencies in C_i clearly correspond to the high-intensity 947 and 967 cm^{-1} IR bands in β. The very intense 883 cm^{-1} IR frequency of C_{2v} likely corresponds to the 915 cm^{-1} IR band of α and to the 913 cm^{-1} IR band of δ. Then, the two somewhat intense 906 and 910 cm^{-1} IR frequencies of C_{2v} appear as a single IR band at 944 cm^{-1} in α and as two IR bands at 930 and 941 cm^{-1} in δ. The low-intensity 828 and 862 cm^{-1} IR frequencies in C_i seem to correspond to the low-intensity 832 and 872 cm^{-1} IR bands in β, although the first IR frequency is less intense than the second one in C_i, whereas the first IR band is more intense than the second one in β.

The correspondence between the four low-intensity IR frequencies of C_{2v} (828, 836, 864, and 869 cm^{-1}), the three IR bands of α (847, 864, and 878sh cm^{-1}), and the three IR bands of δ (830sh, 841, and 864 cm^{-1}) is not as straightforward. If the most intense of these low-intensity IR bands in C_{2v}, α and δ (836, 847, and 841 cm^{-1}), all correspond to the same molecular motion, then three things are true: (1) the 828 cm^{-1} IR frequency of C_{2v} corresponds to the 830sh cm^{-1} IR band of δ and does not appear in α, (2) the 864 cm^{-1} IR frequency of C_{2v} corresponds to the 864 cm^{-1} IR band of α and the 867 cm^{-1} IR band of δ, and (3) the 869 cm^{-1} IR frequency of C_{2v} corresponds to the 878sh cm^{-1} IR band in α and does not appear in δ.

With the exception of the 925 cm^{-1} Raman frequency, whose motion is concentrated in ν(NN) and the rocking of CH_2 moieties on the CH_2 plane, denoted ρ(CH_2), all the frequencies of C_i in this region involve C−N stretching of the C_4N_4 ring. References 2, 4, and 5 assigned general ring-stretching motion to all the IR and Raman bands of β in this region. Hence, the calculated motion of the frequencies of C_i is in agreement with the previously proposed assignments for the IR and Raman bands of β in this region, except for the Raman frequency of C_i at 925 cm^{-1}, which may correspond to the Raman bands at 950 and 953 cm^{-1} reported in refs 4 and 5, respectively, for β. Our calculated frequencies of C_i agree within 8−29 and 8−30 cm^{-1} with the Raman bands of β reported in refs 4 and 5. Similarly, all the frequencies of C_{2v} in this region involve C−N stretching of the C_4N_4 ring, with the exception of the frequency at 910 cm^{-1}, whose motion is concentrated in the NO_2 moieties as ν(NN) and b(ONO). References 2 and 4 assigned general ring stretching to all the IR and Raman bands of α and δ in this region. Hence, the calculated motion of the frequencies of C_{2v} agrees with the previously proposed assignments in refs 2 and 4, except for the frequency of C_{2v} at 910 cm^{-1}, which does not involve ring stretching and corresponds to our IR bands at 944 cm^{-1} in α and 941 cm^{-1} in δ. Our calculated Raman frequencies of C_{2v} agree within 9−35 and 6−33 cm^{-1} with the Raman bands of α and δ reported in ref 4.

Region 970−1240 cm^{-1}. In this region, there is an impressive difference in the IR intensity pattern between the first three frequencies of C_i (1057, 1137, and 1213 cm^{-1}) and the first three frequencies of C_{2v} (989, 1062, and 1097 cm^{-1}). In C_i, these frequencies have monotonically increasing IR intensities, whereas in C_{2v}, these frequencies have monotonically decreasing IR intensities. This difference is also present in the experimental IR spectra and definitely distinguishes β from α and δ because the first three bands in β (1088, 1146, and 1204 cm^{-1}) have monotonically increasing IR intensities, whereas the first three frequencies in α (1030, 1089, and 1109 cm^{-1}) and the first three

frequencies in δ (1016, 1087, and 1109 cm^{-1}) have monotonically decreasing IR intensities. This IR intensity decrease is more noticeable in α than in δ. The next higher IR frequency in C_i, 1236 cm^{-1}, correlates with the 1239 cm^{-1} IR band in β. The next two higher IR frequencies in C_{2v}, 1207 and 1223 cm^{-1}, appear as a single IR band at 1215 cm^{-1} in α and as two IR bands at 1204 and 1222 cm^{-1} in δ. The 1150 cm^{-1} frequency of C_{2v} is not IR active and has virtually no Raman activity, but it seems to correspond to the weakly resolved IR shoulder at 1148 cm^{-1} in α and at 1147 cm^{-1} in δ. Perhaps this is due to intermolecular hydrogen bonding interactions present in the crystal lattice. As shown in Table 2, the Raman frequencies of C_i agree with the Raman bands of β reported in ref 4 within 1−29 cm^{-1} and with those reported in ref 5 within 3−27 cm^{-1}.

The motion of both the IR and Raman frequencies of C_i in this region is concentrated in the stretching of N−N and C−N bonds. This is in agreement with the assignments reported in refs 2, 4, and 5, except for their assignment of the highest band in this region in both of their IR and Raman spectra of β. They assigned the highest IR and Raman bands to the symmetric stretching of NO_2 moieties, denoted $\nu_s(NO_2)$, whereas we assign them to the asymmetric stretching of C−N−C bonds in the C_4N_4 ring, denoted $\nu_{as}(NC_2)$. As shown in Table 3, the Raman frequencies of C_{2v} agree within 8−41 and 2−30 cm^{-1} with the Raman bands of α and δ reported in ref 4. Of the six frequencies of C_{2v} in this region, the first five are concentrated in the stretching of the C_4N_4 ring, whereas the sixth one (1223 cm^{-1}) involves the stretching of only one N−O bond in NO_2 moieties, denoted ν(NO), plus the stretching of N−N bonds and the bending of C−N−C angles. References 2 and 4 assigned general ring stretching to the IR and Raman bands of α and δ in this region, except for the highest band in the IR and Raman spectra. They assigned the highest band in the IR and Raman spectra of α and δ in this region to the symmetric stretching of two N−O bonds in the NO_2 moieties, denoted $\nu_s(NO_2)$, which is not in agreement with the calculated motion.

Region 1240−1350 cm^{-1}. This region also shows noticeable differences in the IR spectra of C_i and C_{2v}. Concurrently, there are differences in the experimental IR spectra that clearly distinguish β from α and δ. The IR spectral differences between α and δ are more subtle but nevertheless recognizable. In this region, β has the most intense band in its entire IR spectrum at 1279 cm^{-1}, with a shoulder at 1296 cm^{-1}, followed by two low-intensity bands at 1325 and 1349 cm^{-1}. In contrast, the IR spectrum of α in this region shows two closely spaced bands with high intensity at 1259 and 1268 cm^{-1} followed by a sharp intense band at 1319 cm^{-1}. The IR spectrum of δ in this region differs from that of α because the bands in δ are broader, with overlapping intensities and shoulders, giving the impression of poorer band resolution. Specifically, δ has a broad, intense IR band at 1249 cm^{-1} with a shoulder at 1257 cm^{-1}, followed by a slightly more intense band at 1274 cm^{-1} with a shoulder at 1290 cm^{-1} and a less intense band at 1320 cm^{-1} with a shoulder at 1341 cm^{-1}. The IR spectrum of C_i in this region has two high-intensity frequencies at 1280 and 1294 cm^{-1} and two low-intensity frequencies at 1323 and 1347 cm^{-1}. The frequency at 1280 cm^{-1} is the most intense frequency in the entire IR spectrum of C_i and probably corresponds to the most intense band in the IR spectrum of β: the band at 1279 cm^{-1}. In this region, the four IR frequencies of C_i closely resemble the IR bands of β both in frequency magnitude (within 2 cm^{-1}) and in IR intensity pattern.

The way the IR spectrum of C_{2v} differs from that of C_i is that C_{2v} has interspersed high- and low-intensity frequencies in this region. The intense 1251 and 1275 cm^{-1} IR frequencies of C_{2v} are separated by a 24 cm^{-1} frequency interval, which is larger than the 14 cm^{-1} separation between the intense 1280 and 1294 cm^{-1} IR frequencies of C_i. We also see a 25 cm^{-1} frequency separation between the intense 1249 and 1274 cm^{-1} IR bands of δ, which is larger than the 17 cm^{-1} separation between the intense 1279 and 1296 cm^{-1} IR bands of β. This trend suggests that the 1251 and 1275 cm^{-1} IR frequencies of C_{2v} correspond to the 1249 and 1274 cm^{-1} IR bands of δ. Because the separation between the intense 1259 and 1268 cm^{-1} IR bands of α is only 9 cm^{-1}, it seems unlikely that the 1275 cm^{-1} IR frequency of C_{2v} corresponds to the 1268 cm^{-1} IR band of α. Therefore, we assign the 1269 cm^{-1} IR frequency of C_{2v} to the 1268 cm^{-1} IR band of α and assume that the 1275 cm^{-1} IR frequency of C_{2v} is either not manifest in α or may correspond to the unresolved IR shoulder at about 1280 cm^{-1} in α (note that, as shown in Table 3, ref 2 reported an IR band at 1280 cm^{-1} in α). If this is true, then the low-intensity 1293 cm^{-1} IR frequency of C_{2v} does not appear in α but does appear in δ as a well-resolved IR shoulder at 1290 cm^{-1}. The 1327 and 1339 cm^{-1} IR frequencies of C_{2v} appear as a single IR band at 1319 cm^{-1} in α and at 1320 and 1341 cm^{-1} in δ.

There are eight frequencies of C_i in this region (Table 2); four of these are IR-active, and four are Raman-active. Because the four IR frequencies of C_i so neatly resemble the four IR bands of β in both frequency magnitude (within 2 cm^{-1}) and intensity pattern, we can confidently assign the calculated motion of the four IR frequencies of C_i to the four IR bands of β in this region. We also note that the Raman frequencies of C_i agree within 4 cm^{-1} with the Raman bands of β reported in refs 4 and 5. Of the four IR frequencies of C_i in this region, two have $\nu_s(NO_2)$ motion, and two have $\gamma(CH_2)$ motion (i.e., torsion of CH_2 moieties). Similarly, of the four Raman frequencies of C_i in this region, two have $\nu_s(NO_2)$ motion, and two have $\gamma(CH_2)$ motion. This is not in agreement with the assignments made in refs 2, 4, and 5 where only $\nu_s(NO_2)$ motion was assigned to all the IR and Raman bands of β in this region. The motion of each of the eight frequencies of C_{2v} in this region (Table 3) is concentrated in either $\nu_{as}(NC_2)$, $\nu_s(NO_2)$, or $\gamma(CH_2)$. This is not in agreement with the assignments previously proposed in refs 2 and 4 where only $\nu_s(NO_2)$ motion was assigned to all the IR and Raman bands of α and δ in this region.

Region 1350−1500 cm^{-1}. In this region, the IR spectrum of β is also clearly different from that of α and δ. In β, we see a very sharp intense IR band at 1385 cm^{-1} with a shoulder at 1395 cm^{-1}, followed by two sharp bands at 1433 and 1462 cm^{-1}. In α, we see an IR band at 1370 cm^{-1} with shoulder at 1364 cm^{-1}, a more intense band at 1393 cm^{-1} with shoulder at 1386 cm^{-1}, a low-intensity band at 1414 cm^{-1}, and a sharp, higher-intensity band at 1451 cm^{-1}. In δ, we see three IR bands (1370, 1383, and 1395 cm^{-1}) with monotonically increasing intensity, a 1419 cm^{-1} band, and a more intense 1451 cm^{-1} band with a shoulder at 1440 cm^{-1}. The four IR frequencies of C_i in this region correspond to the four IR bands of β. In both C_i and β, the first IR band is more intense than the second one, and the third IR band is less intense than the fourth. However, the first IR band in β, 1385 cm^{-1}, has a relatively large intensity, being the second most-intense band in the entire IR spectrum of β, whereas the first IR frequency in C_i, 1397 cm^{-1}, has a rather low intensity. Because the motion of this band is concentrated in the CH_2 moieties (see discussion following), it is possible that intermolecular hydrogen bonding, which is not included in the calculation but is certainly present in the crystal lattice, may be responsible for such IR intensity enhancement

of the 1385 cm^{-1} band in β relative to the IR intensity of the 1397 cm^{-1} band in C_i.

If we assume that the most intense IR bands of C_{2v} in this region, 1404 and 1454 cm^{-1}, correspond to the 1393 and 1451 cm^{-1} IR bands of α and the 1395 and 1451 cm^{-1} IR bands of δ, then the less intense 1382, 1387, and 1423 cm^{-1} IR frequencies of C_{2v} may correspond to the 1370, 1386sh, and 1414 cm^{-1} IR bands of α and the 1370, 1383, and 1419 cm^{-1} IR bands of δ. Then the 1433 and 1447 cm^{-1} IR frequencies of C_{2v} do not appear in α but do appear in δ as an IR shoulder at 1440 cm^{-1}.

The motions of the eight frequencies of C_i in this region are clearly divided into two separate groups. The motion of the first four frequencies is concentrated in the wagging of H atoms out of the CH_2 plane, denoted $\omega(CH_2)$, whereas the motion of the next four frequencies is concentrated in the bending of H−C−H angles, denoted b(HCH). These calculated motions of the CH_2 moieties are consistent with the assignments previously proposed in refs 2, 4, and 5 where a general deformation of CH_2 moieties was assigned to all IR and Raman bands of β in this region. However, we hasten to point out that the motion of the CH_2 moieties of C_i in this region does not include torsions, denoted $\gamma(CH_2)$. Similarly, the motions of the 10 frequencies of C_{2v} in this region are concentrated in the CH_2 moieties as $\omega(CH_2)$, $\gamma(CH_2)$, and b(HCH). This is consistent with the previous assignments made in refs 2 and 4 where all the IR and Raman bands of α and δ in this region were assigned to general CH_2 deformations. When the calculated frequencies are compared with the experimental Raman spectra in this region, we see that the Raman frequencies of C_i agree within 8 cm^{-1} with the Raman bands of β reported in refs 4 and 5 and that the Raman frequencies of C_{2v} agree within 14 and 11 cm^{-1} with the Raman bands of α and δ reported in ref 4.

Region 1500−1700 cm^{-1}. In this region, both IR spectral plots of C_i and C_{2v} show only two closely spaced intense frequencies separated by 11 and 3 cm^{-1}, respectively. The experimental IR spectra also show two intense bands separated by 29 cm^{-1} in β, 34 cm^{-1} in α, and 17 cm^{-1} in δ. There also appear to be additional shoulders in the experimental IR spectra that are not present in the calculated spectra. Furthermore, the two IR frequencies in C_i are 81 and 63 cm^{-1} higher than the corresponding IR bands in β. The first IR frequency in C_{2v} is 23 cm^{-1} higher than the first IR band in α and is 19 cm^{-1} higher than the first IR band in δ, whereas the second IR frequency in C_{2v} is 8 cm^{-1} lower than the second IR band in α and is 5 cm^{-1} higher than the second IR band in δ. Therefore, it seems that intermolecular hydrogen-bonding effects play a significant role in the separation and location of these two IR bands. This seems to be particularly exemplified in β, where pronounced intermolecular hydrogen bonding afforded by the β lattice may be responsible for drastically lowering the frequency of these two bands.

There are four frequencies of C_i in this region. Two of these four frequencies are IR-active and two are Raman-active. The motion of all four frequencies of C_i is localized in asymmetric stretches of the NO_2 moieties, denoted $\nu_{as}(NO_2)$. There are also four frequencies of C_{2v} in this region, and all four have $\nu_{as}(NO_2)$ motion. This is in agreement with the $\nu_{as}(NO_2)$ assignment previously proposed for all of the IR and Raman bands of α, β, and δ in this region.[2,4,5]

Region 2900−3100 cm^{-1}. The IR spectra of α, β, and δ show unique features in this region, distinguishing among phases. The IR spectrum of β shows low-intensity bands at 2925, 2985, and 2992 cm^{-1} and two high-intensity bands at 3027 and 3037 cm^{-1}, with the last band being the most intense. The IR spectrum of α shows a low-intensity band at 2970 cm^{-1} and two intense bands at 3049 and 3056 cm^{-1}, with the next-to-last band (3049 cm^{-1}) being the most intense. The IR spectrum of δ shows bands that are proper for δ, plus additional low-intensity bands with frequency values reminiscent of the bands in β. This suggests that the δ sample contained a small remnant of the parent β phase, from which the δ sample was obtained by heating. The IR bands proper for δ appear to consist of a low-intensity shoulder at 2970 cm^{-1} and an intense band at 3058 cm^{-1} with an unresolved lower-frequency shoulder, whereas the low-intensity IR bands caused by remnant β are 2925, 2992, 3027, and 3037 cm^{-1}.

Because this is a region where Fermi resonances may cause bands to split and shift, we group the IR bands in this region into two categories—those below 3000 cm^{-1} and those above 3000 cm^{-1}— to compare them with the calculated frequencies. The frequency separation between the highest IR frequency below 3000 cm^{-1} and the lowest IR frequency above 3000 cm^{-1} is smaller in C_i than in C_{2v}. Similarly, this frequency separation is smaller in β than in α and δ. Furthermore, the IR frequencies that are above 3000 cm^{-1} in C_i are lower than those frequencies in C_{2v}, and similarly, those in β are lower than those in α and δ. We also note that the highest IR intensities in C_i and C_{2v} occur below 3000 cm^{-1}, whereas the highest IR intensities in α, β, and δ occur above 3000 cm^{-1}.

As shown in Tables 2 and 3, in this region, there are eight frequencies in C_i and eight frequencies in C_{2v}, with their molecular motions entirely localized in the stretching of C−H bonds. This is in agreement with the previously proposed assignment of C−H bond stretching for all of the IR and Raman bands of α, β, and δ in this region.[2,4,5] In both C_i and C_{2v}, the IR and Raman frequencies below 3000 cm^{-1} are symmetric C−H stretches, denoted $\nu_s(CH_2)$, and frequencies above 3000 cm^{-1} are asymmetric C−H stretches, denoted $\nu_{as}(CH_2)$. With this region, we conclude our scrutiny of the calculated and measured spectra.

In the energy distribution analysis, the molecular motions (bond stretches, bends, and torsions) corresponding to each vibrational frequency are expressed in terms of redundant internal valence coordinates. This analysis showed that at higher frequencies, such as $\nu_{as}(NO_2)$ and $\nu_{as}(CH_2)$, the motions of both C_i and C_{2v} conformations of the $H_8C_4N_8O_8$ molecule seemed very localized in coordinates that describe functional groups. However, motions of lower frequencies, such as ring distortions, were diffusely distributed among several types of coordinates involving various atoms. A notable exception to this trend of diffuse motion at lower frequencies was the torsions of the four NO_2 groups, denoted as $\gamma_{NN}(NO_2)$ in Tables 2 and 3. They are among the lowest frequencies, yet they are very localized, that is, they are not strongly coupled to the rest of the molecule. This exception is important because torsional motions have been thought of as doorways through which kinetic energy can flow into the molecule from its surroundings. This notion is based on the assumption that the torsional motions of the molecule's functional groups are usually highly coupled to the rest of the molecule.[26]

Table 4 shows the calculated energies of the $H_8C_4N_8O_8$ molecule at the optimized geometries of the chair and boat conformations. The chair conformation (C_i symmetry) is only slightly more stable than the boat conformation (C_{2v} symmetry), by 1.94 kcal/mol. Whereas this is consistent with the fact that β is the most stable polymorph at room temperature, such a small energy difference cannot, by itself, account for the

TABLE 4: Energies of the $H_8C_4N_8O_8$ Molecule in the C_i and C_{2v} Conformations

conformation[a] symmetry	absolute energy (hartrees)	zero-point[b] energy (kcal/mol)	relative energy (kcal/mol)
C_i	−1196.545957	118.35	0.00
C_{2v}	−1196.542456	118.09	1.94

[a] Conformers shown in Figure 1a and b. [b] Values scaled by 0.9806 as recommended in ref 27.

preferred stability of β. Hence, we suspect that intermolecular hydrogen bonding enhanced by the particular packing of $H_8C_4N_8O_8$ molecules in the chair conformation in the β-phase lattice also contributes to the stability of β. This notion is consistent with the fact that the $\nu_{as}(NO_2)$ bands in β are drastically lower (up to 81 cm^{-1}) than those in C_i because the O···H intermolecular hydrogen bonding between the NO_2 moieties of one $H_8C_4N_8O_8$ molecule and the CH_2 moieties of the neighboring $H_8C_4N_8O_8$ molecules is present in the lattice but is not included in the calculation.

V. Conclusions

We have presented a quantum mechanical study of the vibrational spectra of the $H_8C_4N_8O_8$ molecule in C_i and C_{2v} symmetry conformations in the gas phase. We used molecular calculations that are based on density functional theory and the SQM force-field method, with the constant scaling factors of Baker and colleagues.[20] These constant scaling factors, originally developed for molecules in the gas phase, were also useful in our analysis of the vibrational spectra of the α, β, and δ crystal lattices of HMX. The calculated frequencies were generally in good agreement with the experimental bands, within 41 cm^{-1}.

Our analysis of the vibrational spectra verifies that the particular conformation of the $H_8C_4N_8O_8$ molecule in each crystal lattice of HMX determines, to a great extent, the general pattern of the vibrational spectrum of the crystal lattice. In the β phase, where the $H_8C_4N_8O_8$ molecules are in the chair conformation with C_i symmetry, the experimental IR spectrum resembles the calculated spectrum of the $H_8C_4N_8O_8$ molecule with C_i symmetry in the gas phase. Similarly, in the α and δ phases of HMX, where the $H_8C_4N_8O_8$ molecules are in the boat conformation and are slightly distorted from C_{2v} symmetry by each lattice, the experimental IR spectra resemble the calculated IR spectrum of the $H_8C_4N_8O_8$ molecule with C_{2v} symmetry in the gas phase.

By comparing the similarities between calculated and measured IR spectral plots, we attempted to establish a one-to-one correspondence between calculated and measured bands, thereby assigning the intermolecular motion of the calculated frequencies to the measured bands. On the basis of these detailed assignments, we were able to confirm many of the general assignments that had been proposed in previous experimental IR and Raman spectroscopic work on HMX polymorphs. In addition, the calculated motions allowed us to question some of these previously proposed assignments and to offer new assignments consistent with our calculations.

We found good agreement between the calculated geometry of the $H_8C_4N_8O_8$ molecule in the C_i symmetry conformation and the experimental geometry of $H_8C_4N_8O_8$ molecules in the β-phase lattice of HMX. We also found good agreement between the calculated geometry of the $H_8C_4N_8O_8$ molecule in the C_{2v} symmetry conformation and the experimental geometry of $H_8C_4N_8O_8$ molecules in the α- and δ-phase lattices of HMX. If we consider that the calculated geometric parameters are for a molecule in the gas phase, whereas the experimental geometric parameters are from molecules in crystal lattices, then the overall good agreement between the calculated and experimental geometric parameters is encouraging.

Acknowledgment. This work is supported by the U.S. Department of Energy. We thank all of the previous and current members of the High Explosive Reaction Chemistry by Ultrafast Laser Excited Spectroscopies project for their helpful and enthusiastic comments. We also thank Dr. Jon Baker for technical assistance.

Supporting Information Available: Dihedral angles of the $H_8C_4N_8O_8$ molecule in C_i and C_{2v} conformations are listed in Table 1S. This material is available free of charge via the Internet at http://pubs.acs.org.

References and Notes

(1) Cady, H. H.; Smith, L. C. *Los Alamos Scientific Laboratory Report LAMS-2652 TID-4500*, Los Alamos National Laboratory: Los Alamos, NM, 1961.
(2) Goetz, F.; Brill, T. B.; Ferraro, J. R. *J. Phys. Chem.* **1978**, *82*, 1912.
(3) Yoo, C.-S.; Cynn, H. *J. Chem. Phys.* **1999**, *111*, 10229.
(4) Goetz, F.; Brill, T. B. *J. Phys. Chem.* **1979**, *83*, 340.
(5) Iqbal, Z.; Bulusu, S.; Autera, J. R. *J. Chem. Phys.* **1974**, *60*, 221.
(6) Sorescu, D. C.; Rice, B. M.; Thompson, D. L. *J. Phys. Chem. B* **1998**, *102*, 6692−6695.
(7) Kohno, Y.; Uida, K.; Imamura, A. *J. Phys. Chem.* **1996**, *100*, 4701−4712.
(8) Dlott, D. D.; Fayer, M. D. *J. Chem. Phys.* **1990**, *92*, 3798.
(9) Tokmanoff, A.; Fayer, M. D.; Dlott, D. D. *J. Phys. Chem.* **1993**, *97*, 1901.
(10) Tarver, C. M. *J. Phys. Chem. A* **1997**, *101*, 4845.
(11) Cady, H. H.; Larson, A. C.; Cromer, D. T. *Acta Crystallogr.* **1963**, *16*, 617.
(12) Choi, C. S.; Boutin, H. P. *Acta Crystallogr., Sect. B* **1970**, *26*, 1235.
(13) Cobbledick, R. E.; Small, R. W. H. *Acta Crystallogr., Sect. B* **1974**, *30*, 1918.
(14) *International Tables for Crystallography*, 3rd ed.; Hahn, T., Ed.; Kluwer Academic Publishers (published for the International Union of Crystallography): Boston, MA, 1992; Vol. A.
(15) Hehre, W. J.; Radom, L.; Schleyer, P. v. R.; Pople, J. A. *Ab Initio Molecular Orbital Theory;* Wiley-Interscience: New York, 1986; p 82.
(16) Becke, A. D. *J. Chem. Phys.* **1992**, *97*, 9173. Becke, A. D. *J. Chem. Phys.* **1993**, *98*, 5648.
(17) Stephens, P. J.; Devlin, F. J.; Chablowski, C. F.; Firsch, M. J. *J. Phys. Chem.* **1994**, *98*, 11623.
(18) Lee, C.; Yang, W.; Parr, R. G. *Phys. Rev. B* **1988**, *37*, 785.
(19) Frisch, M. J.; Trucks, G. W.; Schlegel, H. B.; Scuseria, G. E.; Robb, M. A.; Cheeseman, J. R.; Zakrzewski, V. G.; Montgomery, J. A., Jr.; Stratmann, R. E.; Burant, J. C.; Dapprich, S.; Millam, J. M.; Daniels, A. D.; Kudin, K. N.; Strain, M. C.; Farkas, O.; Tomasi, J.; Barone, V.; Cossi, M.; Cammi, R.; Mennucci, B.; Pomelli, C.; Adamo, C.; Clifford, S.; Ochterski, J.; Petersson, G. A.; Ayala, P. Y.; Cui, Q.; Morokuma, K.; Malick, D. K.; Rabuck, A. D.; Raghavachari, K.; Foresman, J. B.; Cioslowski, J.; Ortiz, J. V.; Stefanov, B. B.; Liu, G.; Liashenko, A.; Piskorz, P.; Komaromi, I.; Gomperts, R.; Martin, R. L.; Fox, D. J.; Keith, T.; Al-Laham, M. A.; Peng, C. Y.; Nanayakkara, A.; Gonzalez, C.; Challacombe, M.; Gill, P. M. W.; Johnson, B. G.; Chen, W.; Wong, M. W.; Andres, J. L.; Head-Gordon, M.; Replogle, E. S.; Pople, J. A. *Gaussian 98*, revision A.4; Gaussian, Inc.: Pittsburgh, PA, 1998.
(20) Baker, J.; Jarzecki, A. A.; Pulay, P. *J. Phys. Chem. A* **1998**, *102*, 1412.
(21) Ma, B.; Lii, J.-H.; Schaefer, H. F., III; Allinger, N. L. *J. Phys. Chem.* **1996**, *100*, 8763.
(22) Rauhut, G.; Pulay, P. *J. Phys. Chem.* **1995**, *99*, 14572.
(23) Diaz-Acosta, I.; Baker, J.; Cordes, W.; Pulay, P. *J. Phys. Chem. A* **2001**, *105*, 238.
(24) Pulay, P.; Torok, F. *Acta Chim. Acad. Sci. Hung.* **1966**, *47*, 273.
(25) *SCALE*; Parallel Quantum Solutions: Fayetteville, AR.
(26) Kirin, D.; Volovsek, V. *J. Chem. Phys.* **1997**, *106*, 9505.
(27) Scott, R. P.; Radom, L. *J. Phys. Chem.* **1996**, *100*, 16502.